Journal of Nuclear Materials 467 (2015) 398–405

Contents lists available at ScienceDirect

Journal of Nuclear Materials

journal homepage: www.elsevier.com/locate/jnucmat

New interatomic potentials for studying the behavior of noble gas atoms in tungsten

Fen Zhou [a], Jingzhong Fang [a], Huiqiu Deng [a, *], Jianglong Liu [a], Shifang Xiao [a], Xiaolin Shu [b], Fei Gao [c], Wangyu Hu [a]

[a] Department of Applied Physics, School of Physics and Electronics, Hunan University, Changsha 410082, China
[b] Department of Physics, School of Physics and Nuclear Energy Engineering, Beihang University, Beijing 100191, China
[c] Department of Nuclear Engineering and Radiological Sciences, University of Michigan, Ann Arbor, MI 48109, USA

HIGHLIGHTS

- New potentials for W–He, W–Ne and W–Ar interactions were developed.
- The "s-band model" was used to describe the many-body interactions.
- The binding energies of an X atom to X_n or X_n–Vacancy clusters were obtained.
- The migration energies of X atoms and X clusters were discussed.

ARTICLE INFO

Article history:
Received 5 February 2015
Received in revised form
6 May 2015
Accepted 7 May 2015
Available online 14 May 2015

ABSTRACT

To study the behavior of noble gas atoms (He, Ne and Ar) in bulk tungsten, new DFT-based potentials for W–He, W–Ne and W–Ar interactions were developed by fitting the results obtained from density functional theory calculations. The new potentials adopt the embedded atom method (EAM) formalism, and the "s-band model" is used to describe the many-body interactions between each of the noble gas atoms and its neighboring W atoms. These potentials reproduce the formation energies of point defects and the migration barriers of single noble gas atoms. The simulations using these potentials successfully predict that the tetrahedral interstitial site is more stable than the octahedral interstitial site for X (= He, Ne or Ar) interstitials. Based on these new potentials, the binding interactions of a single X atom with the X_n and X_n–Vacancy clusters and the diffusion properties of X_n clusters in bulk W were studied using molecular dynamics (MD) simulations. The present results indicate that the binding energies obtained using the new potentials are good in agreement with the results of DFT calculations. The migration energies of the clusters increase with both the increase in the atomic radius of noble gases and the increase in the size of the clusters.

1. Introduction

The plasma-facing materials (PFMs) in fusion devices will be subjected to extreme environments, such as heavy heat load, high energy neutrons and high flux H/He plasma bombardment. Tungsten (W) is considered to be one of the most promising candidate PFMs due to its high melting point, high thermal conductivity and low sputtering characteristics [1,2]. Recently, Takamura et al. [3] found for the first time that deeply nanostructured tungsten (or "fuzz") with an arborescent shape was formed on tungsten-coated graphite via high-flux He plasma irradiation. This structure was demonstrated to greatly change the physical properties of the W surface such as the heat transfer, fuel (deuterium/tritium) retention and erosion rates, which severely impact the operation of fusion devices [4–8]; therefore, it is very important to understand the formation mechanism of fuzz on the surface. To date, various mechanisms have been advocated to explain the formation of such nanostructures experimentally and theoretically. Krasheninnikov [9] presented a viscoelastic model of W fuzz growth that the formed bubbles promoted the flowing of W atoms from the base to

* Corresponding author. Tel.: +86 731 88823226.
E-mail address: hqdeng@hnu.edu.cn (H. Deng).

http://dx.doi.org/10.1016/j.jnucmat.2015.05.004
0022-3115/

the surface, which finally resulted in the formation of a nano-fiber. Kajita et al. [10] considered that the pinholes on the surface and the over-pressured He bubbles resulted in the formation of nanowires. Sefta et al. [11,12] suggested that the accumulation of surface adatom islands resulting from single self-interstitial migration, bubble bursting and prismatic loop punching were responsible for the initial stages of fuzz formation. Hu et al. [13] studied the trap mutation and dissociation of He clusters in the near-surface region of tungsten, which has significant impact on the W surface morphology and near-surface structure. More recently, Sandoval et al. [14] have studied the growth process of He bubbles in W and found that the evolution of surface morphology is very sensitive to the growth rate of He bubbles. The above studies imply that He bubbles are necessary for the initiation of fuzz formation in W bulk.

Both Ne and Ar are noble gas elements and they were also found to form bubbles in materials, such as Si and PtSi [15–17]. Ne and Ar gases are usually introduced into the fusion Tokamaks as coolants [18]. Many properties of Ne and Ar are in common with He, however, the fiber-formed nanostructures were not formed on the W surface by exposure to Ar or Ne plasmas [18], even under the irradiation condition that W nanostructures were formed by He plasma irradiation. Furthermore, Takamura and Miyamoto [19] observed that the pre-existing fibers on W surface were eliminated after they were treated with Ar plasma. The different influence on W surface microstructure caused by He, Ne and Ar plasma irradiation is receiving more attention recently. The penetration depth, which impacts the distribution of noble gas bubbles, has been studied by experiments and binary-collision-approximation-based simulation [18,20]. The results indicated that He atoms, even with lower incident energy, can penetrate into a deeper position than Ne and Ar, which implied that He atoms had a higher probability to cluster in the deeper area far away from the surface. The bubbles at various depths caused different degrees of damage to the surface microstructure and the sufficient penetration (several atomic layers) under the sputtering energy was a necessary condition for the formation of fiber nanostructures [11,20]; therefore, the shallow penetration depth of Ne and Ar under the sputtering energy was one of the reasons why the nanostructures failed to form on W surface by Ne and Ar plasma irradiation [18]. The clustering and growth mechanisms of bubbles also play an important role in the formation of nanostructures. Based on the results of various W–He empirical potentials, it can be found that the binding and diffusion properties of He cluster are very critical in forming bubbles [21–25]. Due to the lack of the interatomic potentials for W–Ne and W–Ar, these properties of Ne or Ar interstitials and clusters in W bulk have not been studied up to now. Based on first-principles density functional theory (DFT) results, three new Embedded-atom method (EAM) potentials for W–X (X = He, Ne, or Ar) were developed in the present study. First, these potential parameters were fitted and validated carefully. Next, these potentials were used to predict the most stable interstitial sites for X atoms, to calculate the binding energies of an X atom additional to X_n and X_n–V clusters, and to discuss the diffusion properties of single X atoms and X_n clusters.

2. Methodology

2.1. The interatomic potentials of W–He, W–Ne and W–Ar

To study the properties of noble gas atoms in the bulk and surface of tungsten, the interatomic potentials (W–W, He–He, Ne–Ne, Ar–Ar, and W–X) are required for performing the atomic-scale simulations. Here and in the following, "X" indicates the noble gas atom He, Ne or Ar. More than 30 potentials for W have been published in the literature, as mentioned in a recent review paper [26]. In the present study, the 'EAM2' potential for W constructed by Marinica et al. [27] was chosen to describe the interactions between W atoms, which was validated by Bonny et al. [26] as one of the most appropriate potentials for describing the properties of extended defects in line with DFT data (qualitatively or quantitatively). To minimize the errors, the same HFD-B-type pair potentials presented by Aziz et al. [28–30] were used to describe the interactions of He–He, Ne–Ne and Ar–Ar. Based on the Hartrec–Fock-Dispersion (HFD) potential, an additional parameter was added into the HFD-B potential, where not only the Hartrec–Fock repulsion but also the dispersion interaction had been taken into considered [31–33].

The potentials for W–X are based on the EAM formalism, which is the same as that of the W–W potential presented in [27]:

$$E(r_1,\ldots,r_N)=\sum_{i=1}^{N}\left[\sum_{j>i}^{N}V(r_{ij})+F_s(\rho_i)\right]. \tag{1}$$

Here E, $V(r)$ and $F_s(\rho)$ are the total energy, pair potential and many-body interaction (or embedding function), respectively. The pair potential $V(r)$ is described by a summation of cubic knot functions

$$V(r)=\sum_{k=1}^{9}a_k(r_k-r)^3H(r_k-r), \tag{2}$$

where $H(r_k-r)$ is the Heaviside function. The many-body interaction $F_s(\rho)$ for W–X is given as follows:

$$F_s(\rho_i)=b_1\sqrt{\rho_i}+b_2\rho_i^2, \tag{3}$$

where ρ_i is the electron density in position i. $F_s(\rho)$ is the sum of the contributions of the electron densities from the surrounding W and noble gas atoms. The parameters b_1, b_2, a_k and r_k ($k=1$–9) are determined by fitting to the first-principles DFT data.

The noble gas X atoms have closed-shell electronic structures, and the bonding interaction with the host is weak due to electronic hybridization [34]. The hybridization of the electron density between the interstitial X atoms and its nearest-neighboring W atoms has been verified by first-principles DFT calculations [35]. For the new W–X potentials, the many body interactions contributed by the hybridization of the electron density were described by the "s-band model", which has the same scheme as the "Two-band model" [36]. In our previous papers, the "s-band model" was successfully used to describe the many-body interactions of Fe–He [37] and Er–He [38]. According to the "s-band model", the Slater function is used to handle the mixed-pair electron density:

$$\rho_s=\sum\Phi_s, \tag{4}$$

$$\Phi_s^{\mathrm{W-He}}=N_s r^5\exp(-2\xi_s), \tag{5}$$

$$\Phi_s^{\mathrm{W-Ne}}=N_s r^6\exp(-2\xi_s), \tag{6}$$

$$\Phi_s^{\mathrm{W-Ar}}=N_s r^7\exp(-2\xi_s). \tag{7}$$

Here, N_s is chosen to be 20.0. ξ_s is an average ξ (Slater orbital exponent) from the 1 s/2 s/3 s and 6 s Hartree–Fock orbitals for He/Ne/Ar and W [39,40]. To attain a higher fitting precision, ξ_s was adaptively adjusted.

2.2. Fitting database and approach for the potential parameters

He, Ne and Ar interstitials are quite insoluble in W because of the large solution energies [35]. Single X atoms usually occupy the tetrahedral interstitial site (TIS), octahedral interstitial site (OIS), or substitutional site (SS) in W bulk. To obtain the parameters of the W–X potentials, the formation energies of the point defects, the binding energies of X–X atoms, and the corresponding atomic configurations of the X atoms in W bulk are chosen as the fitting data obtained by the first-principles DFT calculations. The formation energy (E_f) of one X atom or X_nV_m cluster in W bulk can be calculated by

$$E_f(X_nV_m) = E_{tot}(X_nV_m) - \left(nE_X^C + (N-m)E_W^C\right), \quad (8)$$

where N is the total number of W atoms in a perfect crystal, and n and m are the numbers of X atoms and vacancies (V) in a X_nV_m cluster, respectively. $E_{tot}(X_nV_m)$ is the total energy of the system containing one X_nV_m cluster. E_X^C and E_W^C represent the cohesive energies of X in gases and bcc W crystal, respectively.

The binding energy (E_b) of an X atom to another X atom or an X_nV_m cluster can be obtained by

$$E_b(X) = E_f(X) + E_f(X_nV_m) - E_f(X_{n+1}V_m), \quad (9)$$

where $E_f(X)$ is the formation energy of a single X interstitial in the W bulk. When n and m are equal to 1 and 0, respectively, E_b is the binding energy between two X atoms. In Section 3.2, Eq. (9) is used to calculate the binding energies of an X atom to X_n clusters and X_nV clusters. According to this expression, the formation energies of these clusters must be calculated. However, for large clusters, the most stable configurations are difficult to find because the X atoms in the clusters are arranged in random ways; therefore, in this study, thousands of those configurations with X atoms located at different positions in the clusters are generated and then fully relaxed to a minimum of potential energy by molecular statics with quick-min method. The configuration with the lowest formation energy is considered as the most stable one.

Similar to the Fe–He system [37], the parameters of W–X potentials are fitted by the least squares method

$$U = \sum w_i[f_i(\lambda) - F_i]^2, \quad (10)$$

where U is the objective function, and F_i is the fitting data obtained from our DFT results. The initial values are given to the fitting parameters λ. Based on these parameters, MD simulations are operated to calculate f_i in a box of $6a \times 6a \times 6a$ with 432 W atoms, where a is the lattice constant (0.314 nm, obtained from the W potential in Ref. [27]). w_i represents the weight of each of the fitting data. The simulated annealing algorithm and the simplex method are used to search for the potential parameters for which U reaches the local minima.

2.3. Modeling and simulation methods

The DFT calculations in this study are implemented in the Vienna *ab initio* Simulation Package (VASP) [41]. The interactions between ions and electrons are described using the projector-augmented wave (PAW) potentials [42]. The generalized gradient approximation (GGA) with exchange and correlation functional proposed by Perdew and Wang (PW91) are used in the calculations [43]. The plane-wave energy cutoff is set to 500 eV. The fitting data mentioned above are studied in a $4a_0 \times 4a_0 \times 4a_0$ supercell with 128 atoms, where a_0 is the lattice parameter (0.3177 nm) of bcc W bulk. Periodic boundary conditions are adopted in three directions. The Brillouin zones are sampled with $3 \times 3 \times 3$ k-points generated by the Monkhorst–Pack scheme [44]. The convergences are verified with different k-points, plane-wave energy cut-off values and cell sizes during the calculations. All of the fitting data required are listed in Table 1.

Based on the newly developed W–X potentials, MD simulations with MOLDY computer code [45] are used to study the most stable interstitial sites for point defects, the interactions of X atoms with clusters and the diffusion properties of X atoms and X_n clusters in W bulk. A $10a \times 10a \times 10a$ box containing 2000 W atoms is constructed. The NVT ensemble and periodic boundary conditions are used in the present simulations. The velocity scale method is adopted to control the temperature of the system. The migration energies of single X atoms predicted by the present potentials are obtained using two methods: the mean-square displacement

Table 1
The formation energies (E_f) of point defects, the binding energy (E_b) of X–V or X–X atoms and the migration energy (E_m) of a single X (= He, Ne or Ar) atom in bulk W obtained using the DFT and empirical potential (EP) calculations. ΔE_f is the energy difference of the X atom at the OIS and TIS. The energy units are in eV. The diffusion path for the NEB calculation is from one TIS to its nearest neighbor one.

$E_{f,SS}$	$E_{f,TIS}$	$E_{f,OIS}$	ΔE_f	$E_{b,X-V}$	$E_{b,X-X}$	E_m		References
						NEB	MSD	
He								
4.77	6.15	6.37	0.22	4.57	1.02	0.07		Present DFT results
	6.29	6.67	0.38			0.06		Tamura's DFT results [35]
4.70	6.16	6.38	0.22	4.57	1.03	0.06		Becquart's DFT results [48,49]
4.82	6.13	6.25	0.12	4.80	0.75	0.12	0.10	Present EP results
3.63	4.77	4.76	−0.01		0.81		0.24	Wilson's EP results [53]
6.29	8.20	7.94	−0.26		0.82		0.29	Henriksson's EP results [54]
4.70	6.16	6.31	0.15	5.09	0.86	0.21		Juslin's EP results [21]
4.73	6.15	6.38	0.23	4.98	1.66		0.11	Wang's EP results [22]
4.70	6.21	6.39	0.18	5.03	0.63	0.02	0.06	Li's EP results [23]
			0.19	4.55	1.01	0.09		Bonny's EAM1 results [24]
			0.23	4.54	0.51	0.06		Bonny's EAM2 results [24]
Ne								
6.25	11.17	11.70	0.53	8.11	2.29	0.16		Present DFT results
	11.55	12.17	0.62		2.72	0.17		Tamura's DFT results [35]
6.10	11.67	11.94	0.27	9.06	2.23	0.23	0.23	Present EP results
Ar								
9.14	14.55	15.69	1.14	8.60	1.98	0.25		Present DFT results
	14.99	16.05	1.06		1.58	0.19		Tamura's DFT results [35]
9.30	14.58	14.91	0.33	8.77	1.51	0.27	0.27	Present EP results

(MSD) method and the nudged-elastic band (NEB) method [46,47]. The migration energies of X_n clusters are only calculated by the MSD method. By tracking the position $r_i(t)$ of a single X atom or the mass center of an X_n cluster, the MSD is obtained by

$$\mathrm{MSD} = \langle [r_i(t) - r_i(0)]^2 \rangle, \tag{11}$$

where '⟨…⟩' denotes the averaging over all the atoms; then the diffusion coefficient (D) is determined using the Einstein relation equation

$$D = \mathrm{MSD}/6t. \tag{12}$$

According to the Arrhenius's relation of the prefactor (D_0) and activation energy (E_m) of diffusion

$$D = D_0 \exp[-E_m/k_B T], \tag{13}$$

it is obtained that lnD is linearly correlated with $1/T$; thus D_0 and E_m can be estimated by the intercept and slope of the fitted line, respectively.

The NEB method is used to find the minimum energy path (MEP) of an X atom from its initial state to final state. In this study, the initial state and final state refer to one TIS and its nearest neighbor one, respectively. Thirteen images are constructed between them. After the MEP reaches the convergence precision (the residual force on each atom is less than 0.01 eV/Å), the migration energy is determined by the energy of the highest saddle point along the MEP.

3. Results and discussion

3.1. Fitting and validation of the W–X potentials

The results of our DFT calculations are listed in Table 1. The defect formation energies of X atoms at TIS, OIS and SS are obtained first. The formation energies for He, Ne and Ar at TIS are 6.15 eV, 11.17 eV and 14.55 eV, respectively. The energy difference between the TIS and OIS for He, Ne and Ar atoms are 0.22 eV, 0.53 eV and 1.14 eV, respectively, which indicate that the X atoms at TIS are energetically more favorable than those at the OIS. Our DFT results agree well with those of Becquart et al. [48,49] for He atoms in W bulk and also agree reasonably with those of Tamura et al. [35] for He, Ne and Ar atoms in W bulk. With the NEB method, we determined that the migration energy from one TIS to nearest neighbor one was 0.07 eV, 0.16 eV and 0.25 eV for He, Ne and Ar atoms, respectively, and found that an X atom migrated directly along the TIS–TIS path without passing the OIS, which is in consistent with the results of Tamura et al. [35]. The migration energy for He obtained experimentally is 0.24–0.32 eV, which is much higher than DFT results [50,51] and the discrepancy was attributed to the large binding energy between He atoms [49]. The binding energies (E_b) of X–X atoms are found to be 1.02 eV, 2.29 eV and 1.98 eV for He, Ne and Ar atoms, respectively, which imply that Ne interstitials in W bulk have the strongest binding abilities. The binding energies of X–V for He, Ne and Ar are much stronger than X–X atoms, as shown in Table 1. Those results also agree well with those of Becquart et al. [48,49] and Tamura et al. [35].

By fitting to the above DFT results (the formation energies of X defects and the binding energies of X–X atoms) as listed in Table 1, the detailed parameters of the pair potential and the "s-band model" many-body interaction were determined, as presented in Table 2 for He, Ne and Ar atoms, respectively. The curves of the pair potentials, many-body interactions and electron density are shown in Fig. 1. The interactions between W and noble gas atoms clearly increase with increasing atomic radius of the noble gas atoms, especially at the shorter range. Compared with the pair potential of W–X, the contribution of many-body interactions to the total energy is much smaller due to the very low electron densities, but it cannot be ignored here. For studying the radiation effects of the W–X system, the ZBL function should be connected smoothly with the pair potential by a Fermi function at a short range [37,52].

The results obtained using the present and previous empirical potentials (EPs) and DFT calculations are all listed in Table 1 for comparison [21–24,35,48,49,53,54]. Due to the lack of W–Ne/Ar potentials, we only compared the results of the W–He potentials with the results of the other EPs. The W–He potentials constructed earlier have some obvious differences in the calculation of the formation energies of He defects compared to DFT results. The potentials of both Wilson et al. [53] and Henriksson et al. [54] even provided the incorrect favorite site for the interstitial He atom in W bulk. More recently, Juslin and Wirth [21], Wang et al. [22], Li et al. [23] and Bonny et al. [24] significantly improved the results of the W–He potentials. All of these potentials reproduced well the formation energies of the He defects and demonstrated that the He atom at TIS was the most stable configuration in W bulk, which was in good agreement with the results obtained by the DFT calculations [35,48,49]. Predicted by the present W–X potentials, as listed in Table 1, the favorite interstitial site for He, Ne and Ar atoms is the same TIS.

To further validate the present W–X potentials, the diffusion properties of a single X atom and the interactions between X–X atoms have been studied. The diffusion properties are investigated using the NEB method. The minimum migration energies of a single He, Ne and Ar atom migrates from one TIS to the nearest-neighbor one are 0.12 eV, 0.23 eV and 0.27 eV, respectively, which agree well with the results of ours and Tamura's DFT calculations [35]. The results indicate that the migration energies of single X atoms increase with increasing the radius of X atoms. The same conclusion is also obtained via the MSD method, as shown in Section 3.3.

Table 2
Parameters for the W–He, Ne and Ar potentials.

Pair potential								Many-body interaction (s-band model)			
a_k (eV/Å^3)				r_k (Å)							
	He	Ne	Ar		He	Ne	Ar		He	Ne	Ar
a_1	68.164276	26.616738	31.481460	r_1	1.364158	1.323031	1.010000	b_1 (eV Å^{-1})	0.025104	0.079917	0.1803396
a_2	14.281313	78.987917	−31.851694	r_2	1.473713	1.816813	1.050000	b_2 (eV Å^{-4})	1.183700	1.081073	1.3422720
a_3	−2.712702	−52.011158	332.427517	r_3	1.702224	2.102621	1.120157	ξ_s (Å^{-1})	3.235548	3.150047	3.9168382
a_4	−20.09063	49.9919306	144.295805	r_4	1.841117	2.301297	2.187636	N_s (Å^{-1})	20.00	20.00	20.00
a_5	9.8950515	11.6359716	22.7443424	r_5	2.323359	2.476551	2.320271	r_{cut} (Å)	3.94	3.92	3.99
a_6	−1.3911472	−17.556539	−2.9850419	r_6	2.815915	2.637815	2.819555				
a_7	−0.0239992	4.98318030	−0.6523709	r_7	3.012327	2.828261	3.058007				
a_8	0.43256746	−0.0685376	−0.0053067	r_8	3.171508	3.183116	3.171508				
a_9	0.14893734	0.43457101	0.86209432	r_9	3.639649	3.618947	3.687246				

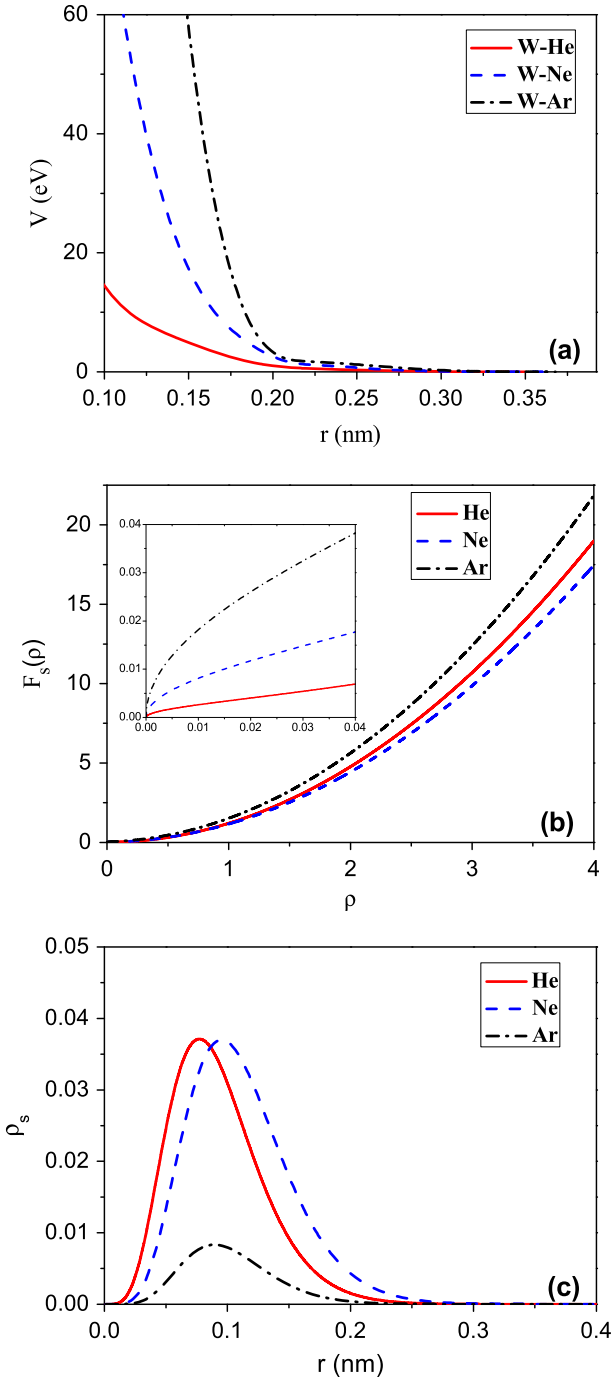

Fig. 1. Pair potentials (a), many-body interaction functions (b) and electron density functions (c) for W–He, W–Ne and W–Ar, respectively.

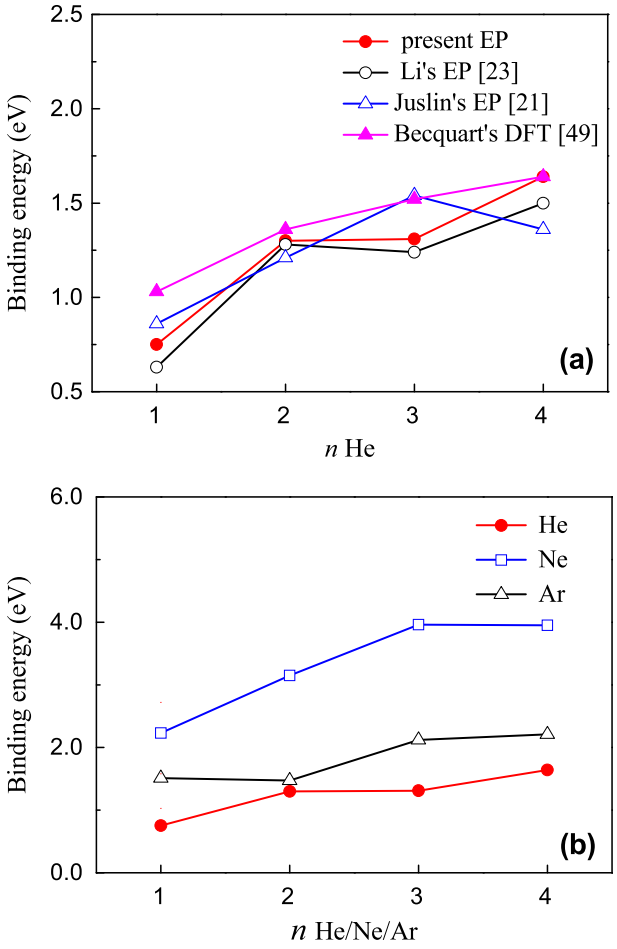

Fig. 2. Binding energies of (a) an additional He atom to a He_n cluster obtained using DFT and different empirical potentials (EP) and (b) an additional X (= He, Ne and Ar) atom to X_n clusters obtained using the present W–X potentials.

Unlike Ne and Ar atoms, the migration properties of single He atoms have been widely studied using various empirical potentials [21–25,55]. The value of E_m for He in W bulk calculated by Juslin and Wirth [21] is 0.21 eV, however, the diffusion path is not specified. Based the Juslin's potential, Wang et al. [55] obtained that the migration energy for He are 0.147 and 0.149 eV via TIS–TIS and TIS–OIS–TIS, respectively which is consistent with the results calculated by Perez et al. [25]. The Julsin's potential slightly overestimate the migration energy compared to the values obtained by the DFT calculations of Becquart and Domain [49] and Tamura et al. [35]. Wang et al. [22], Li et al. [23] and Bonny et al. (EAM2) [24] well predicted the E_m of the interstitial He atom but there was a large discrepancy in the He–He binding energy calculated by these potentials and DFT method [49], as presented in Table 1. Compared with the previous potentials, the present W–He potential not only provides the E_b for dimer He–He more close to the DFT results [49] but also the correct order of stability for interstitial He in W bulk and a reasonable E_m of a single He atom. The binding energies of Ne–Ne and Ar–Ar obtained from the present potentials and the DFT method indicate that the net attractive interactions of Ne–Ne and Ar–Ar are stronger than those of He–He, although the present potentials slightly underestimated the binding energies

3.2. The binding energies of X_n and X_n–V clusters

The binding energies of an additional He atom to He_n clusters were calculated using the present W–He potential, as shown in Fig. 2(a). The results of Juslin and Wirth [21] and Li et al. [23] are also provided here for comparison. The binding energies of the He–He_n clusters calculated by the present W–He potential are 0.75 eV, 1.30 eV, 1.31 eV and 1.64 eV when n equals 1, 2, 3 and 4, respectively, which suggests that the binding energies between a He and He_n clusters increase with the increase in the size of the clusters. The positive binding energies indicate the net attractive interactions between He and He_n clusters. The binding energy of dimer He–He in W bulk calculated by Juslin and Wirth [21] and Li et al. [23] is 0.86 eV and 0.63 eV, respectively, as presented in

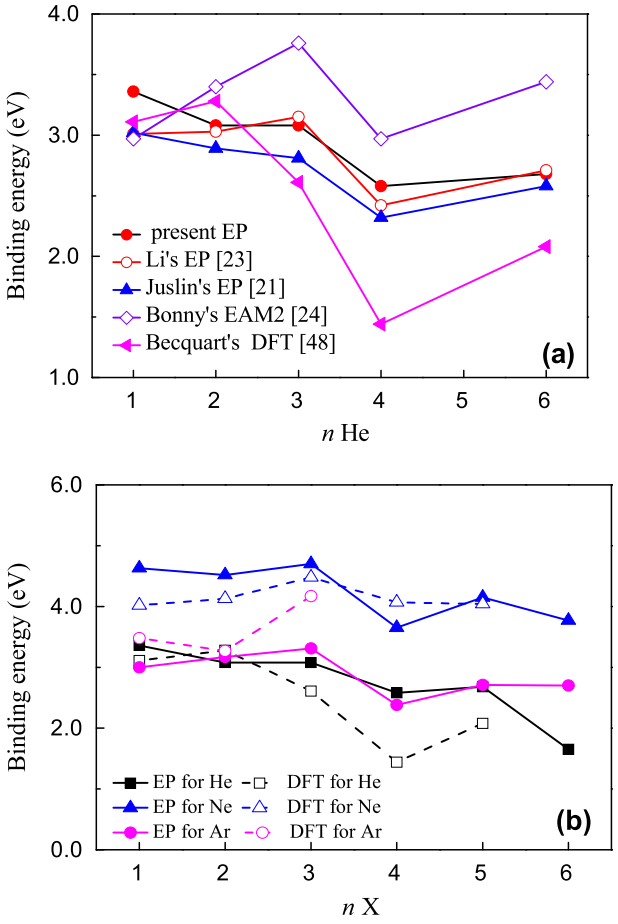

Fig. 3. The binding energies of (a) an additional He atom to He_n–V clusters using different empirical potentials (EP) and (b) an additional X atom to X_n–V clusters obtained using the present W–X potentials and the DFT calculations.

Table 1. Compared with the DFT calculation of Becquart and Domain [49], the three empirical potentials all slightly underestimate the He–He binding energy. However, the He–He_2 binding energies obtained with these empirical potentials agree well with the DFT results. The He–He_3 binding energy calculated by Juslin and Wirth [21] and the He–He_4 binding energy calculated using the present potential are in excellent agreement with the DFT results [49]. Although there are some quantitative differences, the binding energies calculated using these potentials are all in reasonable agreement with the trend of the results of the DFT calculations. Due to the net attractive interactions and very low migration energies of He interstitials, pure He clusters can form without any other defects in metals [56], which is the so-called self-trapping mechanism and makes the He interstitials act as traps for their surrounding He atoms. The binding energies of He_n, Ne_n and Ar_n clusters obtained using the present W–X potentials were compared in Fig. 2(b). The binding energies of Ne_n and Ar_n clusters were also found to increase with the increasing size of the clusters in general. The net attractive interactions between Ne atom and Ne_n clusters are much stronger than the other two noble gas atoms, and the He_n clusters have the smallest binding energies among the three gases. The binding energies of Ne_n clusters are higher than those of He_n and Ar_n clusters, which are within the ranges of 1.48–2.65 eV and 0.72–1.84 eV, respectively, for different n values. Therefore, self-trapping behavior might also occur for Ne and Ar atoms in bulk W, although their migration energies are larger than that of He atoms.

The binding energies of an additional He atom to He_n–V clusters obtained using the present and previous potentials, as well as by the DFT calculations, are plotted in Fig. 3(a). The binding energies are found to decrease with the increase in the size of the He_n–V clusters in general. The positive binding energies indicate the net attractive interactions between He and He_n–V clusters. The binding energies obtained using the present potential are very close to those obtained using the potentials of Juslin and Wirth [21] and Li et al. [23]. Compared with the DFT results of Becquart and Domain [48], these empirical potentials overestimated the binding energies for large He clusters, but the tendencies of the binding energies calculated using these potentials and those determined by the DFT method are basically consistent. The W–He potential of Bonny et al. (EAM2) [24] provides excessively large binding energies compared to the DFT method. The net attractive interactions of the He atom to the He_n–V ($n = 1$–4) clusters calculated using the potentials of the present study, Juslin and Wirth [21] and Li et al. [23] are much stronger than those of the same-sized He_n clusters. This conclusion is also applicable to the DFT results, except for He_4 and He_4–V clusters, because there is a sharp reduction in the He–He_4–V binding energy. The vacancy enhances the binding abilities between single He atoms and clusters. This mechanism is called trap mutation and was first proposed by Caspers et al. [57]. The comparison of the binding energies of the three noble gases calculated using the present potentials and our DFT results is shown in Fig. 3(b). The binding energies of an additional Ne atom to the Ne_n–V clusters exhibit a minor fluctuation in the range of 3.65–4.70 eV but a slightly decreasing trend with increasing size of the clusters. The binding energies calculated using the present W–Ne potential agree with our DFT calculations within 0.61 eV. The net attractive interactions of Ar to the Ar_n–V clusters are smaller than those of the Ne atoms but are very close to those of the He atoms calculated using the present potentials. Although the migration energies of single Ne and Ar atoms are higher than that of He atoms, the stronger binding energies can prompt the occurrence of trap mutation. Compared with pure Ne_n/Ar_n clusters, the net attractive interactions of Ne_n/Ar_n–V clusters with Ne/Ar atoms are stronger for small clusters.

3.3. *The diffusion properties of X atoms and clusters*

To obtain reasonable activation energy, the temperature range was chosen to be from 500 K to 1400 K for the diffusion of X atoms and their clusters in W bulk. Temperatures were avoided at which the clusters would have dissociated, self-interstitial atoms (SIA's) would have been emitted, or at which the clusters would hardly have moved. In the present work, the diffusion properties of single X interstitials and clusters in W bulk were studied using classical MD simulations and MSD analysis. For X clusters, the trajectories of the center of mass were tracked. The diffusivity-temperature curves of a single X atom and X_n clusters are all shown in Fig. 4. The migration energy barriers E_m and the prefactors D_0 obtained using the present and previous potentials are presented in Table 3. From Fig. 4, the diffusion coefficient is found to increase with increasing temperature, which indicates that the increase in temperature promotes the diffusion of X atoms and X_n clusters. A single X interstitial atom can easily change its position when the temperature is high enough. The migration energies of single He, Ne and Ar atoms are 0.098 eV, 0.230 eV and 0.266 eV, respectively. These values are slightly larger than those of the DFT method [35] but agree well with our DFT calculations (as listed in Table 1). The use of the present potentials also successfully predicted that the He atom is the easiest among the three to migrate in W bulk. With the increase in the atomic radius, the diffusion of atoms becomes more difficult.

The same method is also used to study the diffusion of X_n

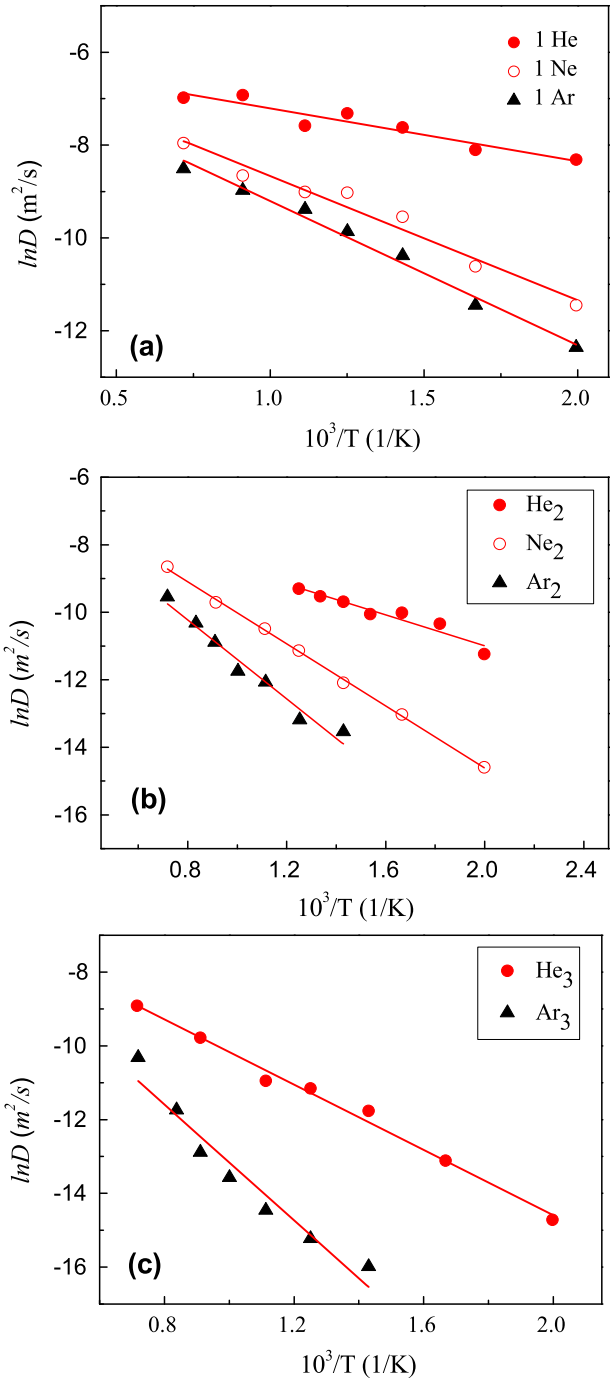

Fig. 4. The lnD–$1/T$ curves of the diffusion of single X atoms and X_n clusters in W.

clusters. An X atom can easily bind with another X atom to form an X_2 cluster due to the large binding energy. For the case of He, the He_2 diffuses as a whole at temperatures below 900 K. When the temperature rises to nearly 900 K, the intense thermal vibrations of He atoms separate the He_2 cluster into two single He atoms. This phenomenon was also observed for He_2 clusters at 900 K by Li et al. [58], but it does not occur in the diffusion process of Ne_2 and Ar_2 clusters. This phenomenon can be explained by the fact that the binding energy of He–He is only 0.75 eV, which is much smaller than those of Ne–Ne and Ar–Ar clusters, as presented in Table 1. The migration energies of He_2, Ne_2 and Ar_2 clusters in W bulk are 0.198 eV, 0.395 eV and 0.503 eV, respectively. Similar to single X atoms, the migration energies of X_2 clusters also increase with the increase in the atomic radius of the noble gas. The migration energy of the Ne_2 cluster is twice as large as that of the He_2 cluster, and the Ar_2 cluster even has a higher migration energy than that of the Ne_2 cluster. The Ar_2 cluster can hardly move at temperatures lower than 700 K. For the three noble gases, the mobility of the atoms is greatly reduced when they become clusters. The He_3 cluster has a larger binding energy than that of He_2 clusters, as shown in Fig. 2(a). The He_3 cluster can diffuse as a whole, even at 1400 K. However, the Ne_3 cluster emits an SIA, leaving a vacancy near the cluster at 500 K or higher temperatures for most of the simulation time; subsequently, the Ne_3 cluster becomes trapped by the vacancy and forms a Ne_3–V cluster. The Ne_3–V cluster is immobile in the W bulk. Therefore, it is very difficult to evaluate the MSD curves for the Ne_3 cluster at temperatures higher than 400 K; as a result, the diffusion coefficient of the Ne_3 cluster is not provided in the present studies. The emission of SIA is also observed in the case of the Ar_3 cluster. Unlike the case of the Ne_3 cluster, the SIA in the Ar_3 cluster can recombine with the vacancy rapidly; this trapping phenomenon is invisible in the MSD curves. The migration energy of the Ar_3 cluster is 0.29 eV larger than that of the He_3 cluster, as presented in Table 3. For small He_n clusters ($n = 1$–3), the potentials of the present study, Li et al. [58] and Perez et al. [25] draw the same conclusion that the migration energies increase with the increase in the clusters' size n. Moreover, the migration energies calculated by the present W–He potential are much closer to the results of Perez et al. [25]. The similar results were obtained by Zhou et al. [59], except for He_2 cluster.

4. Conclusions

New potentials for W–He/Ne/Ar interactions were developed in the present study by fitting the first-principles DFT results. The "s-band model" was used to describe the many-body interactions for the weak electron hybridization between the noble gases and the host W materials. These potentials reproduced well the formation energies of X (= He, Ne or Ar) defects in the W bulk and correctly predicted the most stable TIS interstitial site for the X atom. The binding energies of an additional X atom to the X_n and X_n–V

Table 3
Migration energy barriers (E_m) and prefactor of diffusion (D_0) of X atoms and clusters calculated using the present and previous potentials.

Cluster	E_m (eV)				D_0 (10^{-8} m²/s)		
	Present	Li et al. [58]	Zhou et al. [59]	Perez et al. [25]	Present	Li et al. [58]	Zhou et al. [59]
He	0.10	0.05	0.13	0.15	2.28	3.28	5.35
He_2	0.20	0.11	0.06	0.25	1.64	2.83	0.65
He_3	0.38	0.18	0.23	0.35	3.18	2.36	13.2
Ne	0.23	–	–	–	2.46	–	–
Ne_2	0.40	–	–	–	4.31	–	–
Ar	0.27	–	–	–	2.19	–	–
Ar_2	0.50	–	–	–	3.79	–	–
Ar_3	0.67	–	–	–	4.71	–	–

clusters were calculated; the interactions between the X atom and X_n clusters were found to be attractive, and the presence of a vacancy was found to enhance the binding ability between X atoms and its nearby clusters. The positive binding energies of an additional X atom to the X clusters will increase the possibility of forming X clusters and bubbles through self-trapping and/or trapping mutation mechanisms in W bulk. The results of the study of the diffusion properties of single X interstitials and clusters in W bulk demonstrated that the migration energies of X atoms or clusters increase with the atomic radius of the X atoms and the size of the X clusters. Among these noble gas atoms, He interstitials and clusters diffuse more easily in bulk W. The low migration barriers and high binding energies promote the He atoms forming clusters and bubbles in bulk W.

Acknowledgements

This work was financially supported by the National Natural Science Foundation of China (No. 51371080) and carried out at National Supercomputer Center in Changsha.

References

[1] G. Janeschitz, J. Nucl. Mater. 290 (2001) 1–11.
[2] H. Bolt, V. Barabash, W. Krauss, J. Linke, R. Neu, S. Suzuki, N. Yoshida, A. Team, J. Nucl. Mater. 329 (2004) 66–73.
[3] S. Takamura, N. Ohno, D. Nishijima, S. Kajita, Plasma Fusion Res. 1 (2006) 051.
[4] M.J. Baldwin, R.P. Doerner, W.R. Wampler, D. Nishijima, T. Lynch, M. Miyamoto, Nucl. Fusion 51 (2011) 119501.
[5] K.R. Umstadter, R. Doerner, G. Tynan, Phys. Scr. T138 (2009) 014047.
[6] S. Kajita, S. Takamura, N. Ohno, et al., Nucl. Fusion Res. 47 (2007) 1358.
[7] S. Kajita, N. Ohno, S. Takamura, et al., Appl. Phys. Lett. 91 (2007) 261501.
[8] W. Sakaguchi, S. Kajita, N. Ohno, M. Takagi, J. Nucl. Mater. 390–391 (2009) 1149–1152.
[9] S.I. Krasheninnikov, Phys. Scr. T145 (2011) 014040.
[10] S. Kajita, W. Sakaguchi, N. Ohno, N. Yoshida, T. Saeki, Nucl. Fusion 49 (2009) 095005.
[11] F. Sefta, N. Juslin, B.D. Wirth, J. Appl. Phys. 114 (2013) 243518.
[12] F. Sefta, K.D. Hammond, N. Juslin, B.D. Wirth, Nucl. Fusion 53 (2013) 073015.
[13] L. Hu, K.D. Hammond, B.D. Wirth, D. Maroudas, Surf. Sci. 626 (2014) 21–25.
[14] L. Sandoval, D. Perez, B.P. Uberuaga, A.F. Voter, Phys. Rev. Lett. 114 (2015) 05502.
[15] E. Oliviero, S. Peripolli, L. Amaral, P.F.P. Fichtner, M.F. Beaufort, J.F. Barbot, S.E. Donnelly, J. Appl. Phys. 100 (2006) 043505.
[16] A.G. Cullis, T.E. Seidel, R.L. Meek, J. Appl. Phys. 49 (1978) 5188.
[17] Z.L. Liau, T.T. Sheng, Appl. Phys. Lett. 32 (1978) 716.
[18] M. Yajima, M. Yamagiwa, S. Kajita, N. Ohno, M. Tokitani, A. Takayama, S. Saito, A.M. Ito, H. Nakamura, N. Yoshida, Plasma Sci. Technol. 15 (2013) 282–286.
[19] S. Takamura, T. Miyamoto, Plasma Fusion Res. 6 (2011) 1202005.
[20] S. Saito, A. Takayama, A.M. Ito, H. Nakamura, J. Nucl. Mater. 438 (2013) S895–S898.
[21] N. Juslin, B.D. Wirth, J. Nucl. Mater. 432 (2013) 61–66.
[22] J. Wang, Y. Zhou, M. Li, Q. Hou, J. Nucl. Mater. 427 (2012) 290–296.
[23] X.C. Li, X. Shu, Y.N. Liu, Y. Yu, F. Gao, G.H. Lu, J. Nucl. Mater. 426 (2012) 31–37.
[24] G. Bonny, P. Grigorev, D. Terentyev, J. Phys.: Condens. Matter 26 (2014) 485001.
[25] D. Perez, T. Vogel, B.P. Uberuaga, Phys. Rev. B 90 (2014) 014102.
[26] G. Bonny, D. Terentyev, A. Bakaev, P. Grigorev, D.V. Neck, Modelling Simul. Mater. Sci. Eng. 22 (2014) 053001.
[27] M.C. Marinica, L. Ventelon, M.R. Gilbert, L. Proville, S.L. Dudarev, J. Marian, G. Bencteux, F. Willaime, J. Phys.: Condens. Matter 25 (2013) 395502.
[28] R.A. Aziz, A.R. Janzen, M.R. Moldover, Phys. Rev. Lett. 74 (1995) 1586.
[29] R.A. Aziz, M.J. Slaman, Chem. Phys. 130 (1989) 187–194.
[30] R.A. Aziz, M.J. Slaman, J. Chem. Phys. 92 (1990) 1030.
[31] J. Hepburn, G. Stoles, R. Pcnco, Chem. Phys. Lett. 36 (1975) 451.
[32] R. Ahlrichs, P. Pence, G. Stoles, Chem. Phys. 19 (1977) 119.
[33] R.A. Aziz, H.H. Chen, J. Chem. Phys. 67 (1977) 5719.
[34] X.T. Zu, L. Yang, F. Gao, S.M. Peng, H.L. Heinisch, X.G. Long, R.J. Kurtz, Phys. Rev. B 80 (2009) 054104.
[35] T. Tamura, R. Kobayashi, S. Ogata, A.M. Ito, Model. Simul. Mater. Sci. Eng. 22 (2014) 015002.
[36] P. lsson, J. Wallenius, C. Domain, K. Nordlund, L. Malerba, Phys. Rev. B 72 (2005) 214119.
[37] F. Gao, H. Deng, H.L. Heinisch, R.J. Kurtz, J. Nucl. Mater. 418 (2011) 115–120.
[38] L. Yang, Y.T. Ye, K.M. Fan, H.H. Shen, S.M. Peng, X.G. Long, X.S. Zhou, X.T. Zu, F. Gao, Model. Simul. Mater. Sci. Eng. 22 (2014) 065009.
[39] E. Clementi, C. Rortti, At. Data Nucl. Data Tables 14 (1974) 177–478.
[40] A.D. McLean, R.S. McLean, At. Data Nucl. Data Tables 26 (1981) 197–381.
[41] G. Kresse, J. Hafner, Phys. Rev. B 47 (1993) 558 ibid. 49 (1994) 14251.
[42] G. Kresse, D. Joubert, Phys. Rev. B 59 (1999) 1758.
[43] J.P. Perdew, J.A. Chevary, S.H. Vosko, K.A. Jackson, M.R. Ederson, D.J. Singh, C. Fiolhais, Phys. Rev. B 46 (1992) 6671.
[44] H.J. Monkhorst, J.D. Pack, Phys. Rev. B 13 (1976) 5188.
[45] https://www.wiki.ed.ac.uk/display/ComputerSim/MOLDY.
[46] G. Mills, H. Jónsson, Phys. Rev. Lett. 72 (1994) 1124.
[47] G. Mills, H. Jónsson, G.K. Schenter, Surf. Sci. 324 (1995) 305.
[48] C.S. Becquart, C. Domain, Nucl. Instrum. Meth. Phys. Res. B 255 (2007) 23–26.
[49] C.S. Becquart, C. Domain, Phys. Rev. Lett. 97 (2006) 196402.
[50] A. Wagner, D.N. Seidman, Phys. Rev. Lett. 42 (1979) 515.
[51] J. Amano, D.N. Seidman, J. Appl. Phys. 56 (1984) 983.
[52] J.P. Biersack, J.F. Ziegler, Instr. Meth. Phys. Res. B 141 (1982) 93.
[53] W.D. Wilson, R.A. Johnson. Rare gases in metals, in: P.C. Gehlen, J.R. Beeler, R.J. Jaffee (Eds.), Interatomic Potentials and simulation of Lattice Defects, Battelle Institute Materials Science Colloquia, Columbus, Ohio, 1972, pp. 375–390.
[54] K.O.E. Henriksson, K. Nordlund, J. Keinonen, D. Sundholm, M. Patzschke, Phys. Scripta T108 (2004) 95.
[55] L.F. Wang, X.L. Shu, G.H. Lu, J. Mater. Res. (2015), http://dx.doi.org/10.1557/jmr.2014.407.
[56] W.D. Wilson, C.L. Bisson, M.I. Baskes, Phys. Rev. B 24 (1981) 5616–5624.
[57] L. Caspers, R. Fastenau, A.V. van, W.H. van, Phys. Stat. Sol. 46 (1978) 541.
[58] X.C. Li, X. Shu, P. Tao, Y. Yu, G.J. Niu, Y.P. Xu, F. Gao, G.N. Luo, J. Nucl. Mater. 455 (2014) 544–548.
[59] Y.L. Zhou, J. Wang, Q. Hou, A.H. Deng, J. Nucl. Mater. 446 (2014) 49.